Journal of Photochemistry and Photobiology A: Chemistry 211 (2010) 89–98

Contents lists available at ScienceDirect

Journal of Photochemistry and Photobiology A: Chemistry

journal homepage: www.elsevier.com/locate/jphotochem

# A density functional theory study on the thermal and photochemical isomerization mechanism of 4,4′-azobenzene disulfonate

Yue Zhu[a], Min Pu[a,*], De-Cai Fang[b], Jing He[a], David G. Evans[a]

[a] State Key Laboratory of Chemical Resource Engineering, Beijing University of Chemical Technology, 15 Beisanhuan Dong Road, Beijing 100029, PR China
[b] College of Chemistry, Beijing Normal University, Beijing 100875, PR China

ARTICLE INFO

*Article history:*
Received 5 August 2009
Received in revised form 20 January 2010
Accepted 27 January 2010
Available online 2 February 2010

*PACS:*
31.15.E–
31.15.ee
82.37.Vb
82.50.–m

*Keywords:*
4,4′-Azobenzene disulfonate
Excited state
Potential energy profile
Photoisomerization mechanism
DFT

ABSTRACT

The isomerization pathways of 4,4′-azobenzene disulfonate in the $S_0$ and $T_1$ states have been studied by using density functional theory (DFT) with B3LYP method at the levels of 6-31G(d,p) and 6-311++G(d,p), respectively. There are two isomerization pathways in the $S_0$ state. One is the inversion of one CNN angle combined with certain degree of rotation around the CN bond, and it is worthy to notice that the potential energy profile includes three sequential transition states. The other pathway is the rotation of CNNC dihedral angle involved inversion of one CNN angle, while the two isomers are connected through the only one transition state. Calculation indicates that the molecular structures at the highest points on the potential energy profiles of two pathways are identical, and the energy barriers are the same, 20.52 kcal/mol. In the $T_1$ state, there exists the rotation pathway (rotation of CNNC dihedral angle) and its energy barrier is 4.11 kcal/mol. In the excited states ($T_1$, $S_1$, $T_2$, and $S_2$), the potential energy profiles of the vertical excitation are obtained by time dependent density functional theory (TD-DFT) at the B3LYP/6-311++G(d,p) level. The photoexcitation at 342 nm results in the reactant molecule populated in the $S_2$ state, but isomerization does not occur directly on the $S_2$ state due to the high energy barrier. It could undergo a rapid relaxation to the minimum of $S_1$ state, and then the isomerization occurs using the inversion or rotation pathway. The results show that the rapid energy redistribution among the various vibrations renders the concentration of such amounts of energy in the inversion coordinate very improbable, while there are two possible photoisomerization pathways by the rotation pathway. The isomerization can easily occur through the $S_0/S_1$ conical intersection and the $S_0$–$T_1$–$S_0$ crossing to reach the product. The primary isomerization pathways for 4,4′-azobenzene disulfonate can go through the inversion and rotation forms in the $S_0$ state and the rotation mechanism in the excited state.



## 1. Introduction

Azobenzene derivatives can undergo reversible photoisomerization under the different wavelength of photoexcitation between *trans* (E) and *cis* (Z) conformations. Interest in this topic has been maintained because azobenzene and its derivatives have potentially applied in a number of key areas such as optical switching and memory storage [1–4], molecular scissors [5], molecular machines [6–9], biochemical activity [10,11] and nanodevices [12]. Tailoring of structures for azobenzene derivatives optimized for specific applications requires a detailed understanding of the photoisomerization process.

Azobenzene derivatives can interconvert by both thermally and photochemically. The isomerization of E isomer to Z isomer for azobenzene (Ab) occurs upon UV light at 365 nm (3.40 eV) and a Z to E isomerization takes place at 420 nm (2.95 eV) [13]. A thermally induced Z to E isomerization readily occurs in the ground state. There are two pathways by which isomerization are thought to take place. The rotation pathway involves an out-of-plane rotation of the CNNC dihedral angle around the NN double bond, and the inversion pathway is formed by increasing the CNN bond angle to 180°. A photochemical mechanism of Ab, involving the inversion pathway in the $S_1$ ($n$–$\pi^*$) state and the rotation pathway in the $S_2$ ($\pi$–$\pi^*$) state, was first proposed more than 20 years ago [14]. At the same time, Monti et al. [15] provided the first theoretical explanation for these isomerization pathways by early ab initio work based on minimal basis set CI calculations, which were successfully applied to explain the most experimental results [16–19]. Most researchers agree that the inversion mechanism dominates in the ground state [15,20–22], but there was a lively debate on which mechanism dominates after excitation to each excited state. The time-resolved fluorescence experiment by Fujino et al. [23,24] revealed that isomerization always occurs in the $S_1$ state regardless of excitation wavelength, and their time-resolved Raman

* Corresponding author. Tel.: +86 1064445393.
*E-mail address:* pumin@mail.buct.edu.cn (M. Pu).

1010-6030/$ – see front matter © 2010 Elsevier B.V. All rights reserved.
doi:10.1016/j.jphotochem.2010.01.014

spectroscopy showed that the NN double bond remained intact after the excitation and therefore provides evidence for the inversion mechanism in the $S_1$ state. The most theoretical conclusions agree that the $n \rightarrow \pi^*$ has a slight inversion barrier and a nearly barrierless rotation pathway [20–22,25–28]. Several researchers have found an $S_1$–$S_0$ conical intersection along the rotation pathway with an CNNC dihedral angle of about 90.0° [22,25–29]. Some theoretical studies show that the thermal isomerization of Ab also may involve the conversion between the singlet and triplet states. The computational results based on CASPT2 method by Cembran and coworkers [29] revealed that the thermal isomerization may take place by the adiabatic rotation mechanism on the $S_0$ PES and the nonadiabatic rotation mechanism via the crossing $S_0$–$T_1$–$S_0$. According to B3LYP calculations [30], the results showed that the potential energy curve of the $T_1$ state had a minimum of 27.8 kcal/mol in the rotated region and thus indicated that photoisomerization of this state can occur along the NN rotation path.

The disubstituted azobenzene derivatives also are good candidates not just for many applications as the azobenzene, but also because their photoisomerization mechanism will be extremely important to illustrate the photoresponsive properties and to design better photochemical materials. Some researchers have devoted to the investigation of the structural, spectral, isomerization of the symmetric disubstituted azobenzene derivatives. As early as 1959, Yeh and Jaffé [31] studied the basicities of the 19 disubstituted derivatives of azobenzene, indicating that the conjugate acid of azobenzene derivatives is not a tautomeric mixture of two compounds. Some studies showed that the substituents on the azobenzenes can significantly affect the photochemical characters and the isomerization behavior. Blevins and Blanchard's [21] experimental and computational data indicated that the symmetric disubstitution of azobenzene plays a significant role in determining the ordering of excited electronic states and the thermal isomerization proceeds by inversion of one N atom and not by NN bond rotation. DFT calculation results by Crecca and Roitberg [22] revealed that the inversion pathway is preferred in the $S_0$ state of azobenzene and its four p-disubstitution derivatives, and the electron donating groups increase the ground state inversion barrier while electron withdrawing groups decrease it. The potential energy surfaces for the $S_1$ and $S_2$ states obtained by using TD-DFT method to compute single point vertical excitation energies for each of the points of that in the $S_0$ state. The calculation results indicated that it was probable through the conical intersection found along the rotation pathway as their primary isomerization mechanism. Schmidt et al. [32] studied the ultrafast photoisomerization of a disubstituted azobenzene (4-nitro-4′-dimethyl aminoazobenzene) by means of femtosecond fluorescence and absorption spectroscopy, which indicated that the character of its excited states were strongly altered by the push–pull substitution on azobenzene, but the two stages among the observed three decay stages were very similar to those of the parent azobenzene. In another report [33], no obvious substituent effect on the photodynamics and photoisomerization was observed by sub-picosecond time-resolved absorption spectroscopy for the isomerization of 4-nitro-4′-methoxy-azobenzene via the $S_1$ state. Using DFT-B3LYP calculations, the thermal isomerization of azobenzene and p-aminoazobenzene were studied by Wang and Wang [34]. Their report indicated that azobenzenes could isomerize along rotation and inversion pathways, respectively. However, the molecular structures for p-aminoazobenzene at the highest points on the potential energy surfaces of CNNC rotation and CNN inversion were identical, so it had reason to believe that the two mechanisms operate simultaneously. In later work, Wang et al. [35,36] described the potential energy profile of the $S_0$ and the $S_1$ state for 4-amino-4′-nitro-azobenzene, 4-amino-4′-cyano-azobenzene and 4-aminoazobenzene on the basis of DFT-B3LYP and CASSCF calculations. These calculations suggested that different electron withdrawing groups (–$NO_2$, –CN) on para-positions can modify the conical intersection lying on the rotation decay pathway. Briquet et al. [37] evaluated the structural parameters and the electronic absorption spectra of three para disubstituted *trans* azobenzene derivatives: 4,4′-Cl, 4,4′-$NO_2$, and 4,4′-$NMe_2$. Moreover, some studies investigated disubstituted azobenzene by sulfonic group. 4-Sulfonic-4′-hydroxy-azobenzene was examined in the solid and solution states by $^{13}C$ and $^{15}N$ NMR spectroscopy [38]. The disubstituted of azobenzene sulfonate anions intercalation nanocomposites prepared by using layered materials had exhibited a high degree of polymeric ordering and advanced physicochemical properties compared with the individual parts [39]. On the molecular level, the difference of property can be related with the potential energy surfaces in different states, which determine the isomerization details of the azo. To the best of our knowledge, there has been no report on the photoisomerization mechanism of azobenzene sulfonate at computational level.

In this work, quantum chemical calculations were used to explore the isomerization mechanism of isolated 4,4′-azobenzene disulfonate (AbS), which bears two sulfonic groups as electron withdrawing substituents in the para-positions. The aim of this study is to find out the most efficient isomerization route according to a detailed study of the $S_0$, $T_1$, $S_1$, $T_2$, and $S_2$ potential energy profiles. The new isomerization forms are presented in this paper, which make us to be more clearly understand the isomerization process of azobenzene derivatives.

## 2. Computational details

All the geometries of the ground state ($S_0$) and the first triplet ($T_1$) excited state were fully optimized by using density functional theory (DFT) with the B3LYP functional and the 6-31G(d,p) basis set. It is noted that the choice of basis set is critical for obtaining stable structures, so the 6-311++G(d,p) basis set was also chosen in the B3LYP calculation. This basis set is added diffuse function, and it is essential for accurately describing the interaction between the two phenyl rings in E isomer. The frequencies of all the species were calculated at the same level to identify the nature of the stationary points, and the zero-point energy (ZPE) corrections for each structure were obtained. To investigate the inversion and rotation pathways of the ground state, the potential energy profile was generated by scanning the CNN angle from 100° to 280° and the CNNC dihedral angle from 20.0° to −220.0° at a 10.0° interval. The potential energy profile of $T_1$ state was also obtained by scanning the CNNC dihedral angle from 80.0° to 280.0° at a 10.0° interval. Time dependent density functional theory (TD-DFT) with the B3LYP functional was used for the excited state calculations as it was found to give reliable results [18,25]. The potential energy profiles in the excited state were obtained by calculating single point vertical excitation energies for each of the points of that in the $S_0$ state. All calculations were performed using Gaussian 03 program [40].

## 3. Results and discussion

### 3.1. Isomerization in the $S_0$ state

#### 3.1.1. Equilibrium geometries of EAbS and ZAbS

The optimized structures of trans-AbS (EAbS) and cis-AbS (ZAbS) are shown in Fig. 1. The main structural parameters related to the azo and sulfonic groups, calculated both at the 6-31G(d,p) and 6-311++G(d,p) level, are presented in Table 1. The bond lengths and angles optimized by the 6-31G(d,p) level are in agreement with the results obtained at the 6-311++G(d,p) level. It shows that the basis set effects might be neglected, however, taking into account the

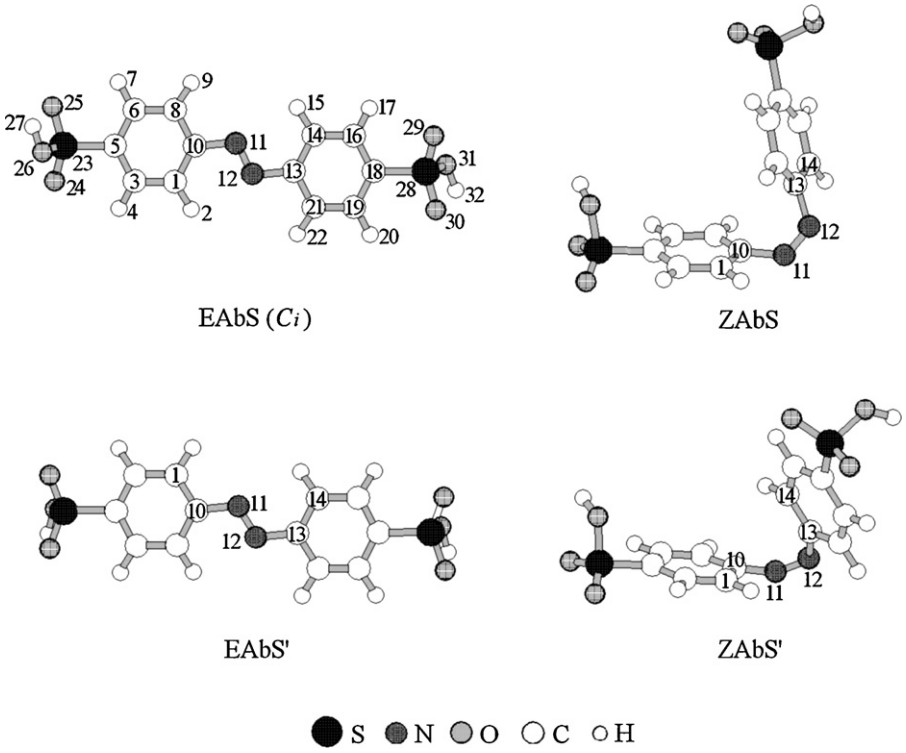


**Fig. 1.** Optimized structures of ABS in the $S_0$ state.

nature of the vertical excitation, all the results and discussions in this paper are obtained at the level of B3LYP/6-311++G(d,p) unless other wise indicated.

For EAbS isomer with $C_i$ symmetry, two phenyl rings are in a plane, and the CNNC dihedral angle is 180.00° while the NNCC dihedral angle is about 0°. ZAbS isomer is nonplanar as the CNNC is 8.88°, and the CCNN is −135.58°. Table 2 provides the energy ($E$), the zero-point energy (ZPE) and the relative energy with respect to the EAbS for all the species. It shows that EAbS isomer is 14.81 kcal/mol lower in energy than ZAbS isomer. Its value very close to the energy gap of azobenzene reported in the literatures [22,34,41], so it is believed that the relative stability of two isomers is not obviously affected by the electron withdrawing substitution.

*3.1.2. Isomerization pathway*

In order to obtain the minimum energy pathway (MEP) in the $S_0$ state, the potential energy profiles were generated by scanning the CNN angle (angle 10–11–12 in Fig. 1) along the inversion pathway and the CNNN dihedral angle (angle 10–11–12–13 in Fig. 1) along the rotation pathway. These calculations showed that each pathway can link the correct products with reactants.

*3.1.2.1. Inversion pathway.* Azobenzene derivatives are known to undergo a thermal Z to E isomerization in the ground state, so only the ZAbS → EAbS barrier will be discussed. The computational energy barrier is 20.52 kcal/mol, which is determined by finding the energy of the transition state and subtracting from it the energy of

**Table 1**
The main geometric parameters of 4,4′-AbS in the $S_0$ state.

| | EAbS | | EAbS′ | | ZAbS | | ZAbS′ | |
|---|---|---|---|---|---|---|---|---|
| | 6-31G(d,p) | 6-311++G(d,p) | 6-31G(d,p) | 6-311++G(d,p) | 6-31G(d,p) | 6-311++G(d,p) | 6-31G(d,p) | 6-311++G(d,p) |
| Bond length (Å) | | | | | | | | |
| C10–N11 | 1.419 | 1.420 | 1.419 | 1.420 | 1.434 | 1.434 | 1.434 | 1.434 |
| N11–N12 | 1.260 | 1.251 | 1.260 | 1.251 | 1.247 | 1.241 | 1.247 | 1.241 |
| N12–C13 | 1.419 | 1.420 | 1.419 | 1.420 | 1.434 | 1.434 | 1.434 | 1.434 |
| C5–S23 | 1.788 | 1.793 | 1.788 | 1.793 | 1.786 | 1.791 | 1.785 | 1.791 |
| S23–O24 | 1.455 | 1.447 | 1.455 | 1.447 | 1.455 | 1.457 | 1.456 | 1.457 |
| S23–O26 | 1.646 | 1.648 | 1.646 | 1.648 | 1.647 | 1.648 | 1.647 | 1.648 |
| O26–H27 | 0.973 | 0.969 | 0.973 | 0.969 | 0.973 | 0.969 | 0.973 | 0.969 |
| Angles (°) | | | | | | | | |
| C10–N11–N12 | 114.59 | 115.13 | 114.57 | 115.16 | 123.85 | 123.71 | 123.97 | 123.89 |
| N11–N12–C13 | 114.59 | 115.13 | 114.60 | 115.12 | 123.92 | 123.78 | 124.03 | 123.94 |
| O24–S23–O25 | 122.21 | 122.71 | 122.02 | 122.69 | 122.06 | 122.75 | 121.67 | 122.71 |
| O25–S23–O26 | 106.47 | 106.99 | 106.41 | 106.91 | 106.41 | 106.93 | 106.47 | 106.89 |
| Dihedral angles (°) | | | | | | | | |
| C1–C10–N11–N12 | −0.13 | 0.20 | 179.91 | −179.74 | −51.79 | −53.05 | −137.21 | −135.58 |
| C10–N11–N12–C13 | −180.00 | −180.00 | 179.93 | 179.86 | −9.69 | −9.20 | 9.55 | 8.88 |
| N11–N12–C13–C14 | 0.15 | −0.20 | 0.21 | 0.27 | −52.42 | −53.92 | −135.92 | −133.87 |
| C3–C5–S23–O25 | −164.35 | −163.31 | −160.84 | −161.07 | −159.59 | −160.23 | −159.59 | −161.83 |
| O25–S23–O26–H27 | 3.62 | −13.90 | 8.48 | −12.75 | 9.22 | −12.24 | 18.51 | −10.99 |

**Table 2**
Energy of all the stationary points for the potential energy profile of the $S_0$ and $T_1$ states.

| | 6-31G(d,p) | | | 6-311++G(d,p) | | |
|---|---|---|---|---|---|---|
| | *E* (a.u.) | ZPE (a.u.) | Δ*E* (kcal/mol) | *E* (a.u.) | ZPE (a.u.) | Δ*E* (kcal/mol) |
| EAbS | −1820.363469 | 0.218656 | 0.00 | −1820.685296 | 0.217400 | 0.00 |
| EAbS′ | −1820.363387 | 0.218611 | 0.02 | −1820.685238 | 0.217394 | 0.03 |
| ZAbS | −1820.339800 | 0.218172 | 14.56 | −1820.661588 | 0.217290 | 14.82 |
| ZAbS′ | −1820.339578 | 0.218056 | 14.63 | −1820.661241 | 0.217183 | 14.97 |
| TS1-inv | −1820.304405 | 0.216368 | 35.66 | −1820.626946 | 0.215354 | 35.36 |
| TS2-E | −1820.353740 | 0.217928 | 5.65 | −1820.677079 | 0.217010 | 4.92 |
| TS2-Z | −1820.334719 | 0.217970 | 17.62 | −1820.656292 | 0.217103 | 18.03 |
| EAbS-$T_1$ | −1820.320549 | 0.216811 | 25.80 | −1820.641746 | 0.215737 | 26.31 |
| ZAbS-$T_1$ | −1820.320549 | 0.216808 | 25.80 | −1820.641746 | 0.215734 | 26.31 |
| TS-$T_1$ | −1820.314007 | 0.216978 | 30.01 | −1820.635324 | 0.215872 | 30.43 |

Δ*E* is the relative energy with respect to the EAbS.

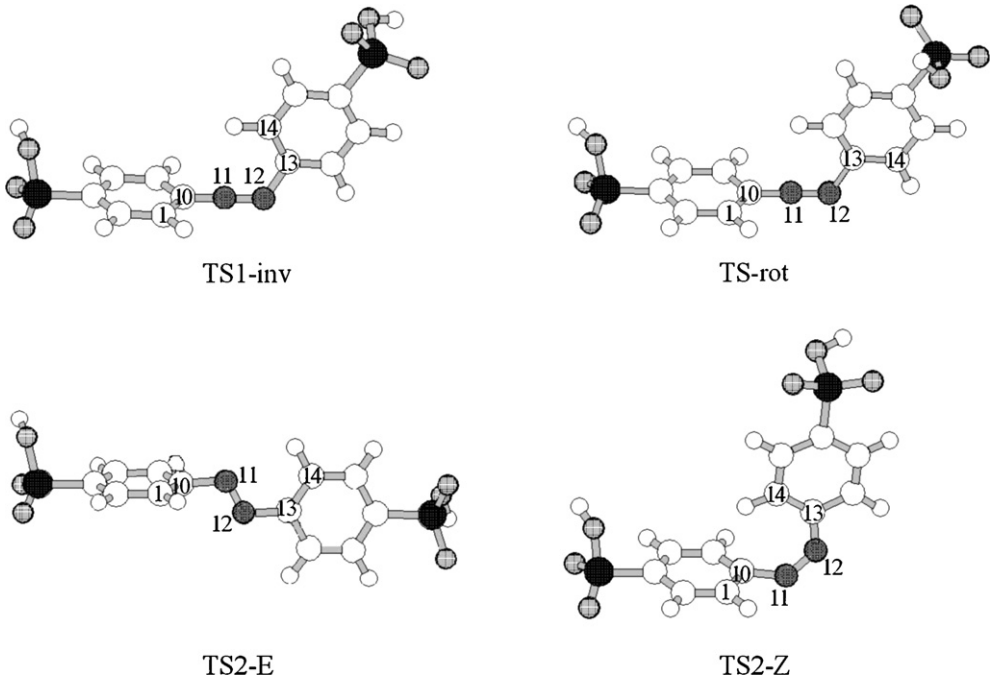


**Fig. 2.** Optimized structures of the transition states of both the inversion and rotation pathways in the $S_0$ state.

the ZAbS minimum. This is just slightly lower than the theoretical value of inversion pathway for azobenzene [22,34], indicating that adding electron withdrawing substituents to the benzene rings of azobenzene decrease the ground state inversion barrier height. As can be seen from Fig. 2, the inversion transition state of the overall reaction from the ZAbS to EAbS is shown and labeled as TS1-inv, and its geometric parameters are shown in Table 3. TS1-inv has only one imaginary frequency, −385 i/cm, which is assigned to the N11 stretching and perpendicular to the inversion phenyl ring. The NN distance in the TS1-inv structure is 1.216 Å, which is shorter than both the Z and E isomers, so the NN double bond stays intact. The geometry of the TS1-inv has lost its symmetry. Especially, the two CNN angles have become different, 179.19° and 117.47°, respectively, and the two NNCC angles are −115.54° and

**Table 3**
The main geometric parameters for TS, II-TS-cis and II-TS-trans in the $S_0$ state.

| | TS-inv | | TS2-Z | | TS2-E | |
|---|---|---|---|---|---|---|
| | 6-31G(d,p) | 6-311++G(d,p) | 6-31G(d,p) | 6-311++G(d,p) | 6-31G(d,p) | 6-311++G(d,p) |
| Bond length (Å) | | | | | | |
| C10–N11 | 1.327 | 1.325 | 1.428 | 1.428 | 1.431 | 1.430 |
| N11–N12 | 1.223 | 1.216 | 1.247 | 1.240 | 1.252 | 1.243 |
| N12–C13 | 1.452 | 1.454 | 1.442 | 1.443 | 1.430 | 1.431 |
| Angles (°) | | | | | | |
| C10–N11–N12 | 179.69 | 179.19 | 126.93 | 127.22 | 113.95 | 114.43 |
| N11–N12–C13 | 117.19 | 117.47 | 126.65 | 126.72 | 114.41 | 115.08 |
| Dihedral angles (°) | | | | | | |
| C10–N11–N12–C13 | 71.29 | 24.63 | −0.18 | −0.16 | 179.98 | 179.82 |
| C1–C10–N11–N12 | −161.66 | −115.54 | −94.65 | −95.23 | 92.31 | 92.23 |
| N11–N12–C13–C14 | 1.22 | 1.03 | 0.24 | 0.41 | −0.32 | −0.73 |

1.03°, respectively. The in-plane inversion of the C10–N11–N12 angle is from 123.79° for ZAbS isomer to an approximate straight line for TS1-inv, and this angle is 114.44° for EAbS isomer. Inversion of C10–N11–N12 angle does not induce the significant change of another N11–N12–C13 angle, only results in a slight compression of the C10–N11 and N11–N12 bonds and the elongation of the N12–C13 bond. As the CNN inversion increases, the transition state corresponds to a linear geometry, and the hybridization of one nitrogen atom changes from $sp^2$ to sp because the coupling between the two nitrogen lone pairs weakens. It is worth noted that the two phenyl rings of TS1-inv are not coplanar, but close to perpendicular to each other. This result indicates that the thermal inversion isomerization process involves the rotation of the phenyl rings.

The inversion potential energy profile is shown in Fig. 3a, which is started from the TS1-inv along the forward and reverse pathway, respectively. Two local minima are obtained on the potential energy profile, and they are neither the ZAbS nor EAbS isomer. The geometries of two minima are fully optimized by using energy gradient technology with the constraint of their symmetry. Surprisingly, both of the optimized geometries are found to have one imaginary frequency, which means that they are transition state on this pathway, and they are labeled as TS2-E (corresponding to the E isomer side) and TS2-Z (corresponding to the Z isomer side). Analyzing the normal mode of imaginary vibration for TS1-inv, it can reach the configuration of TS2-E or TS2-Z followed by the decrease or increase of the CNN angle. It proves that the TS1-inv can link to two transition states by the inversion of the CNN angle. To determine the reactant or product that TS2-E and TS2-Z connect to, the potential energy profiles of these two processes are obtained and shown in Fig. 3b and c, respectively. According to the potential energy profiles, TS2-E is the transition state connecting the two trans-ABS (denoted EAbS and EAbS′, respectively). The structure of EAbS′ is obtained when one phenyl ring of EAbS is rotated 180° around the CN bond, and the two phenyl rings of EAbS′ conformation are approximate planar but with no symmetry. Compared with EAbS, the optimized geometries of EAbS′ show little variation in the NN bond length and most bond parameters, but show obvious variations in the C1–C10–N11–N12 dihedral angle. The energy difference between the EAbS and EAbS′ is 0.03 kcal/mol. Similarly, TS2-Z is linked to two cis-AbS, ZAbS and ZAbS′, respectively. ZAbS′ is also obtained by one phenyl ring rotated around the CN bond, and the energy of ZAbS is 0.15 kcal/mol lower than that of ZAbS′. The energy barrier of EAbS → EAbS′ and ZAbS → ZAbS′ are 4.92 and 3.21 kcal/mol, respectively.

The calculation results reveal that this pathway involves an in-plane inversion of the C10–N11–N12 angle and an out-of-plane rotation around the C10–N11 bond. As can be seen from the schematic diagram in Fig. 4, the entire process of isomerization can be described as follows: the first-order transition state (TS1-inv) of the overall reaction is connected to two transition states by the inversion of the CNN angle, however, both of the transition states can link to two equivalent ZAbS and EAbS, respectively, by the torsion of the CN bond. This isomerization can thus be understood in terms of successive rotation, inversion and rotation processes. There has recently been increasing interest in reactions in which the potential energy profile from one transition state connects not to an intermediate or to a product but to another transition state, which in turn connects two symmetrically equivalent products with lower symmetry. [42,43] Reaction path with sequential transition states is an example of one of the types of phenomena that can occur near a valley-ridge inflection point on a potential energy surface [44]. This new isomerization form, the inversion combined with certain degree of rotation, is different from the previously reported

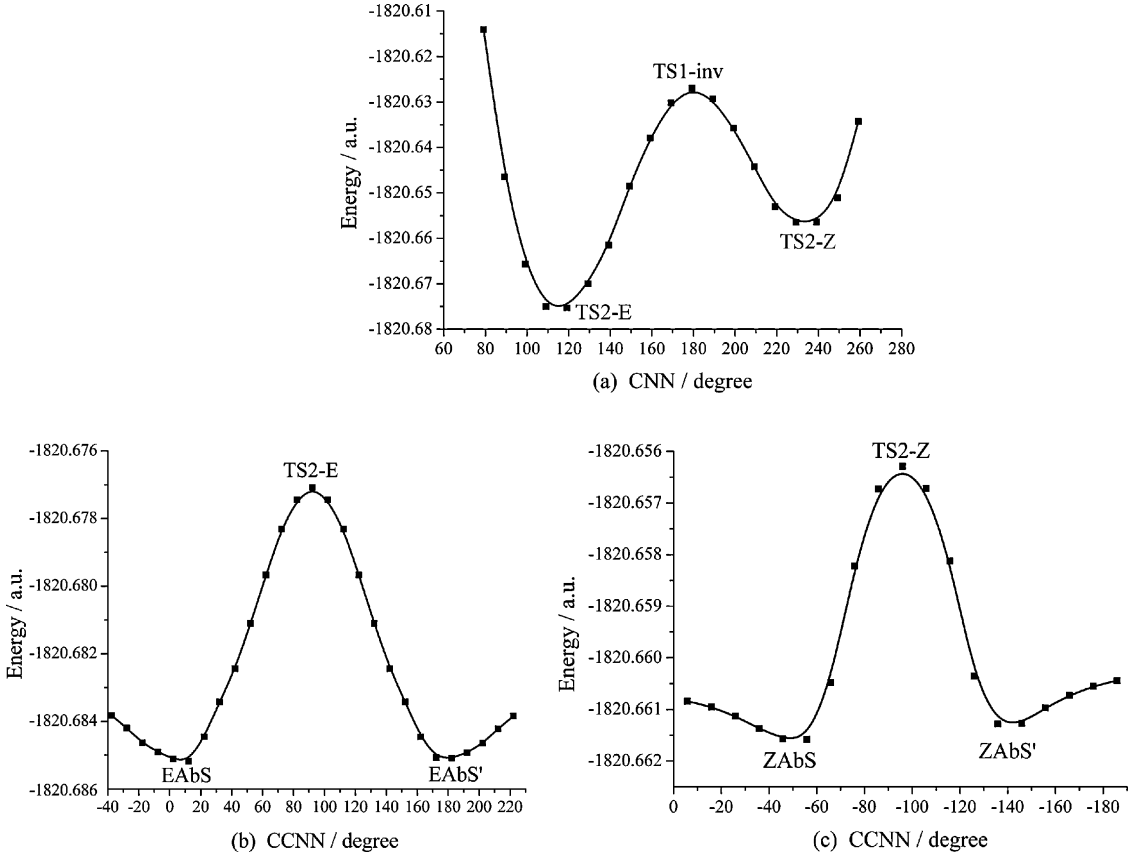


**Fig. 3.** Potential energy profile along the CNN inversion coordinate (a) and CNNC rotation coordinate (b, c) in the $S_0$ state.

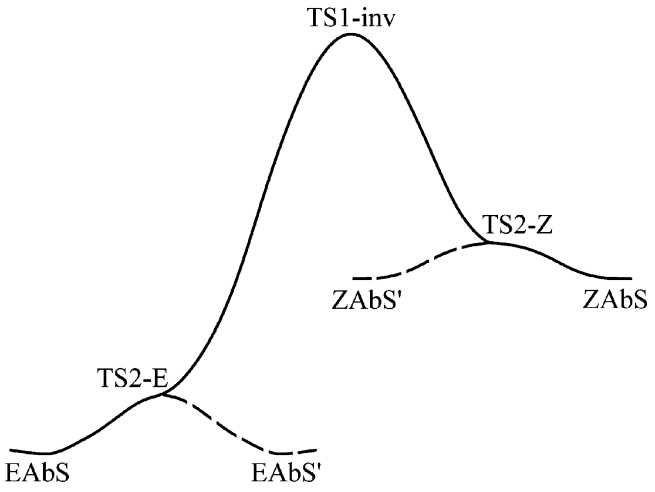


**Fig. 4.** Schematic representation of the inversion pathway in the $S_0$ state, including the second-order transition states.

on the inversion mechanism of azobenzene and its disubstituted derivatives [15,20–22]. For this isomerization process, the TS1-inv structure can only be changed as the CNN inversion increase or decrease because two phenyl rings of AbS molecule needs to keep its symmetry. At the same time, its change is also restricted by two electron withdrawing groups in the symmetrical p-position. Therefore, the two phenyl rings of TS1-inv become orthogonal to each other. Therefore, the thermal inversion isomerization process involves the rotation of the phenyl rings.

*3.1.2.2. Rotation pathway.* The potential energy profile of the C10–N11–N12–C13 dihedral angle rotation is presented in Fig. 5. The geometries and energies of two minima points on this profile are corresponding to the ZAbS and EAbS isomers, respectively. The ZAbS and EAbS isomers are separated by potential energy barriers along the rotation coordinate.

For AbS, the energies and molecular structures of TS-rot and TS-inv appear exceedingly similar (Fig. 2). The NN bond length, CN bond length, CNN angle and one of CCNN dihedral angle of TS-rot are almost the same as those of TS1-inv, while the N11–N12–C13–C14 of both structures are −179.78° and 1.22°, respectively. Optimized the molecular structures at the highest points on the potential energy profiles of CNNC rotation and CNN inversion, the CNN angle of TS-rot is 179.71°, which is very close

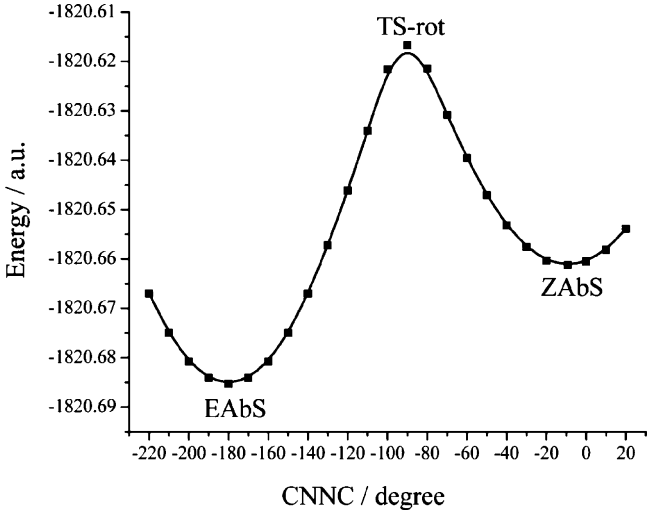


**Fig. 5.** Potential energy profile along the CNNC rotational coordinate in the $S_0$ state.

to the corresponding value of TS1-inv, 179.19°. The planes of two phenyl rings are perpendicular to each other at both structures. However, the above calculation results support the early theoretical finding. Wang and Wang [34] show that the transition states of thermal isomerization for p-aminoazobenzene through inversion and rotation pathways possess the identical molecular structures. For AbS, it was found that the CNN angle changes to 180° rapidly when CNNC dihedral angle changing from 80° to 90° or from 100° to 90°, so this rotation pathway is combined with inversion form. This can be further confirmed by the structural changes in the process of rotation potential energy profile scanning.

For the thermal isomerization of AbS, the inversion pathway is combined with rotation form and the rotation pathway is involved inversion form, so double-pathway mechanism can act simultaneously. The change of the reaction conditions (such as solvent, temperature and pressure) can restrain one of the pathways and promote the other, thus the following studies cannot be excluded that the isomerization occurs possibly by means of the rotation or inversion pathway.

### 3.2. Isomerization in the $T_1$ state

The optimized geometries of the EAbS and ZAbS at the $T_1$ minimum labeled as EAbS-$T_1$ and ZAbS-$T_1$, which are shown in Fig. 6. They are stable at the twisted geometry. According to calculations, following the N = N rotation, the $n \rightarrow \pi^*$ and $\pi \rightarrow \pi^*$ states mix and the weight of the $\pi \rightarrow \pi^*$ component increases, so the molecules become nonplanar. The main structural parameters related to the azo and sulfonic groups are presented in Table 4. There is no remarkable difference between the geometries of the EAbS-$T_1$ and ZAbS-$T_1$ except the C10–N11–N12–C13 dihedral angle, which is −114.25° for EAbS and 114.25° for ZAbS. As can be seen from the data in Table 2, the energies of EAbS-$T_1$ and ZAbS-$T_1$ are almost equal.

The potential energy profile is found to follow the rotation coordinate as shown in Fig. 7. The energy barrier of this isomerization is 4.11 kcal/mol, which is determined by the energy of TS-$T_1$ subtracting from that of the EAbS-$T_1$. The energies and the geometries of two minima points on the potential energy profile are in good agreement with that of EAbS-$T_1$ and ZAbS-$T_1$. The two phenyl rings of TS-$T_1$ are in an approximate planar (see Fig. 6), and the NN double bond still remains throughout the isomerization process. The lowest triplet state shows a still lower energy barrier, so a contribution to the isomerization process may come via the triplet energy curve.

### 3.3. Isomerization in the excited state

#### 3.3.1. Vertical excitation energies of EAbS and ZAbS

For the singlet vertical excitations of EAbS, the first transition, $n \rightarrow \pi^*$, is forbidden and therefore has a very weak oscillator strength, while the second transition, $\pi \rightarrow \pi^*$, is much more intense. Evaluation of their molecular orbitals (see Fig. 8) reveals that the first transition originates from the lone pair on the central nitrogens. The second transition is delocalized throughout the two phenyl rings. For the triplet vertical excitations of EAbS and ZAbS in Table 5, the transition of $T_2 \leftarrow S_0$ and $T_1 \leftarrow S_0$ are forbidden. The excitation energy of EAbS for the $T_2 \leftarrow S_0$ transition is 2.22 eV, corresponding absorption wavelength is at 557 nm. This energy of ZAbS is slightly higher than the EAbS isomer. The $T_1 \leftarrow S_0$ transition for the ZAbS isomer is slightly lower in energy than that of the EAbS isomer.

The lowest vertical singlet excitation energies for these transitions are shown in Table 5. The $\Delta E$ ($S_1$–$S_0$) of EAbS calculated at the 6-311++G(d,p) level for the $S_0$ equilibrium geometry is 2.41 eV. This energy corresponds to the maximum of the $S_1 \leftarrow S_0$ absorption

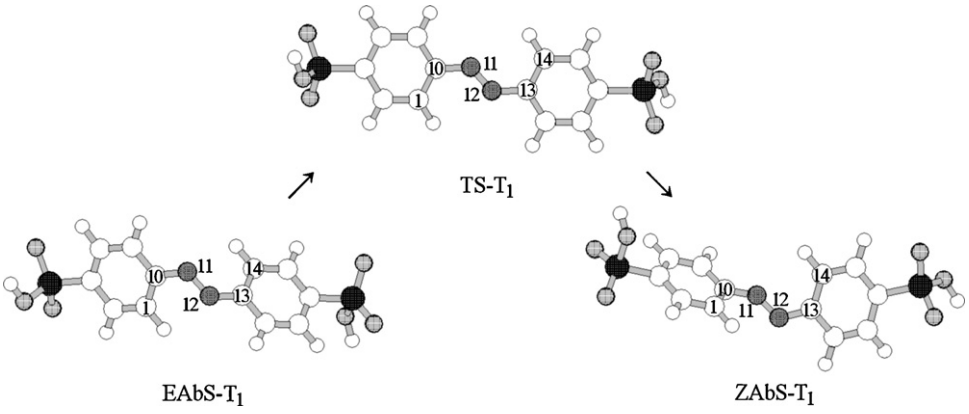


**Fig. 6.** Optimized structures of all the stationary points in the $T_1$ state.

**Table 4**
The main geometric parameters of all the stationary points in the $T_1$ state.

| | EAbS-$T_1$ | | TS-$T_1$ | | ZAbS-$T_1$ | |
|---|---|---|---|---|---|---|
| | 6-31G(d,p) | 6-311++G(d,p) | 6-31G(d,p) | 6-311++G(d,p) | 6-31G(d,p) | 6-311++G(d,p) |
| Bond length (Å) | | | | | | |
| C10–N11 | 1.370 | 1.368 | 1.370 | 1.369 | 1.370 | 1.368 |
| N11–N12 | 1.286 | 1.280 | 1.257 | 1.251 | 1.286 | 1.279 |
| N12–C13 | 1.370 | 1.368 | 1.370 | 1.369 | 1.370 | 1.368 |
| C5–S23 | 1.783 | 1.787 | 1.778 | 1.783 | 1.783 | 1.787 |
| S23–O24 | 1.464 | 1.457 | 1.464 | 1.458 | 1.464 | 1.457 |
| S23–O26 | 1.647 | 1.649 | 1.649 | 1.651 | 1.647 | 1.65 |
| O26–H27 | 0.973 | 0.969 | 0.973 | 0.969 | 0.973 | 0.969 |
| Angles (°) | | | | | | |
| C10–N11–N12 | 123.53 | 123.97 | 128.70 | 128.98 | 123.47 | 123.94 |
| N11–N12–C13 | 123.47 | 123.94 | 128.70 | 128.99 | 123.53 | 123.97 |
| O24–S23–O25 | 122.14 | 122.73 | 121.76 | 122.68 | 122.09 | 122.72 |
| O25–S23–O26 | 106.35 | 106.87 | 106.16 | 106.67 | 106.33 | 106.876 |
| Dihedral angles (°) | | | | | | |
| C1–C10–N11–N12 | −4.02 | −3.85 | −0.28 | −0.19 | 3.84 | 3.72 |
| C10–N11–N12–C13 | 112.50 | 114.25 | 180.00 | 179.98 | −112.49 | −114.25 |
| N11–N12–C13–C14 | −3.84 | −3.72 | 0.28 | 0.19 | 4.03 | 3.86 |
| C3–C5–S23–O25 | −162.07 | −162.57 | −160.01 | −161.86 | −163.09 | −163.33 |
| O25–S23–O26–H27 | 5.68 | −14.19 | 13.86 | −13.6 | 7.59 | −13.07 |

band, which is at 514 nm. The $S_2 \leftarrow S_0$ transition is much better described by TD-DFT with an energy of 3.62 eV, corresponding absorption wavelength is at 342 nm. The $S_1 \leftarrow S_0$ transition occurs at about the similar energy for both EAbS and ZAbS. Unlike the EAbS excitations, however, the $S_1 \leftarrow S_0$ transition for the ZAbS isomer shows slight intensity because of the loss of symmetry making the transition allowed. The $S_2 \leftarrow S_0$ transition for the ZAbS isomer is much less intense and slightly higher in energy than that of the EAbS isomer. As a result of the loss of symmetry (from $C_i$ to no symmetry), it makes to be transformed the forbidden $n \rightarrow \pi^*$ for the EAbS to a slight allowed transition when it converts the EAbS to the ZAbS. Between the ZAbS and EAbS, the $S_2 \leftarrow S_0$ transition is

**Table 5**
Vertical excitation energy of AbS.

| | EAbS[a] | | ZAbS | |
|---|---|---|---|---|
| | 6-31G(d,p) | 6-311++G(d,p) | 6-31G(d,p) | 6-311++G(d,p) |
| $S_2 \leftarrow S_0$ ($\pi \rightarrow \pi^*$) | | | | |
| $E_{ex}$ (eV)[b] | 3.66 (1.08) | 3.62 (1.07) | 4.11 (0.09) | 4.10 (0.09) |
| λ (nm) | 338 | 342 | 302 | 304 |
| $T_2 \leftarrow S_0$ ($\pi \rightarrow \pi^*$) | | | | |
| $E_{ex}$ (eV)[b] | 2.19 (0.03) | 2.22 (0.00) | 3.12 (0.00) | 3.16 (0.00) |
| λ (nm) | 565 | 557 | 397 | 392 |
| $S_1 \leftarrow S_0$ ($n \rightarrow \pi^*$) | | | | |
| $E_{ex}$ (eV)[b] | 2.41 (0.00) | 2.41 (0.00) | 2.52 (0.05) | 2.52 (0.05) |
| λ (nm) | 514 | 514 | 491 | 492 |
| $T_1 \leftarrow S_0$ ($n \rightarrow \pi^*$) | | | | |
| $E_{ex}$ (eV)[b] | 1.67 (0.00) | 1.68 (0.00) | 1.54 (0.00) | 1.57 (0.00) |
| λ (nm) | 743 | 734 | 803 | 790 |

[a] The calculation results show that the $S_1 \leftarrow S_0$ transition of EAbS isomer is Ag $n \rightarrow \pi^*$, and the $S_2 \leftarrow S_0$ transition of that is Au $\pi \rightarrow \pi^*$.
[b] Intensity is in parentheses.

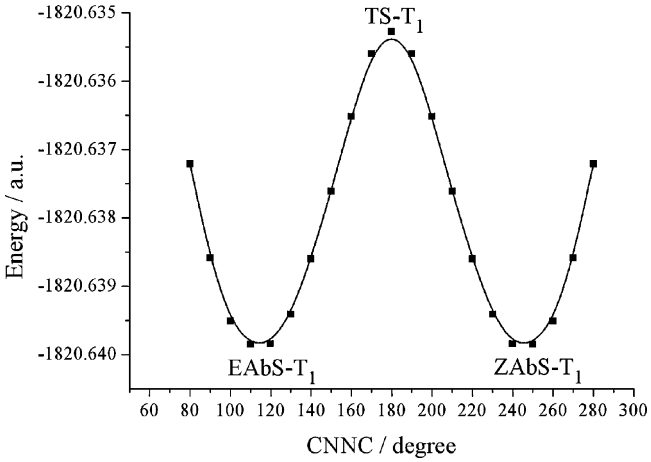


**Fig. 7.** Potential energy profile of $T_1$ state along the CNNC coordinate.

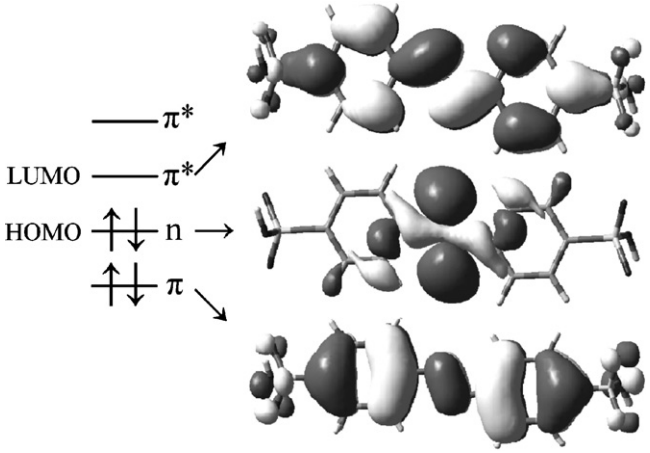


**Fig. 8.** The frontier orbital of EAbS involved in the $S_1 \leftarrow S_0$ and $S_2 \leftarrow S_0$ transitions.

a greater difference than the $S_1 \leftarrow S_0$ transition. The ZAbS isomer shows the much larger energy gap than EAbS.

*3.3.2. Isomerization pathway*

In order to study the photochemical isomerization pathway, the potential energy profiles of the $T_1$, $S_1$, $T_2$, and $S_2$ state along the inversion and rotation pathway were computed.

*3.3.2.1. Inversion pathway.* The excited state potential energy profiles along the inversion pathway are shown in Fig. 9. As can be seen from the data in Table 5, the $S_2 \leftarrow S_0$ excitation is allowed. The $S_2$ potential energy profile along the inversion pathway has only a steep slope above the area corresponding to the EAbS minimum, and the $E \rightarrow Z$ energy barriers is 28.14 kcal/mol, which was determined by finding the energy of the maximum along the inversion of CNN pathway and subtracting from it the energy of the E minimum. The reaction cannot follow the $S_2$ energy profile if excited from the EAbS isomer. However, there is a very flat slope on the ZAbS side. It is without encountering any barrier when excited from the ZAbS isomer to the excited state minimum. There is a steep slope above the area corresponding to either the EAbS or ZAbS minimum on the $T_2$, and the trans → cis energy barriers is 52.03 kcal/mol. There-

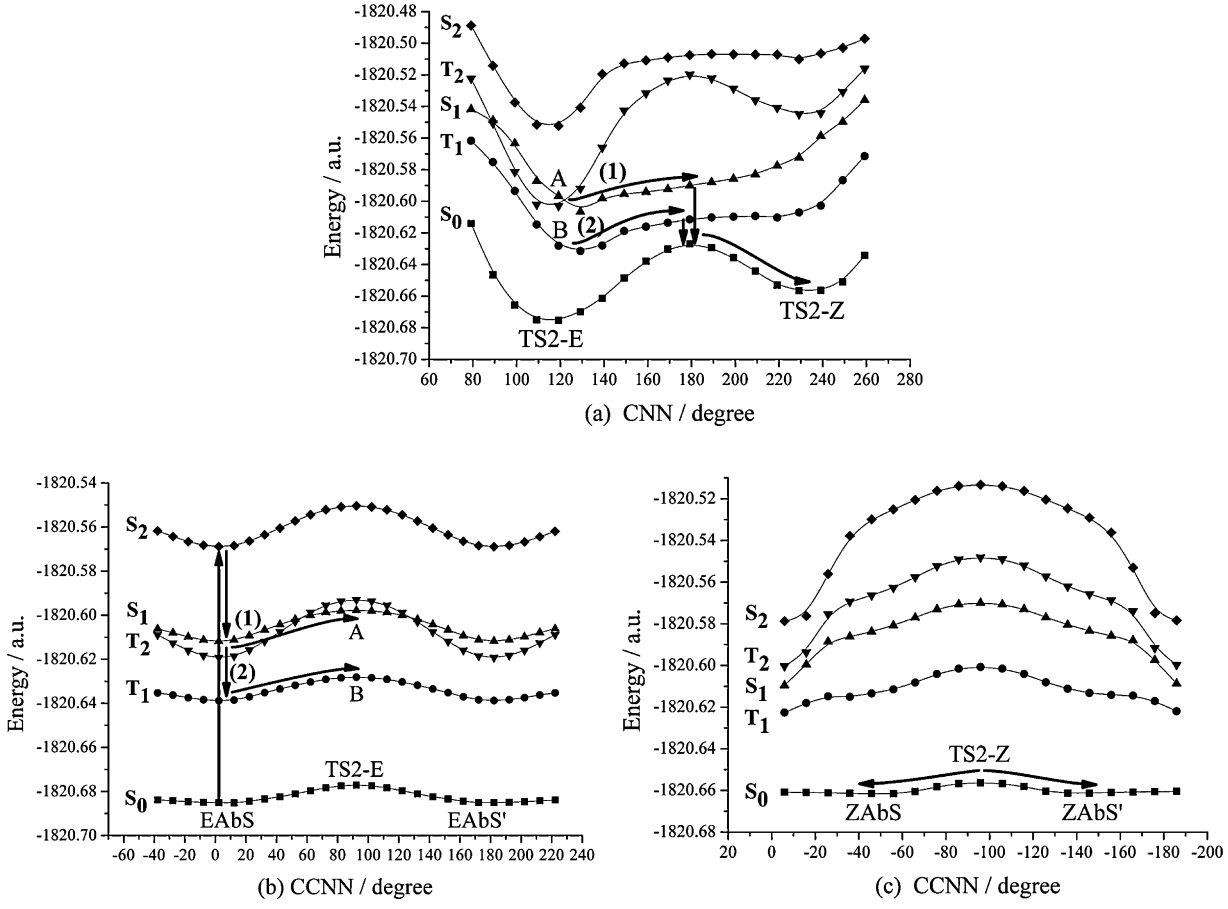


**Fig. 9.** Potential energy profile of the excited state along the CNN inversional coordinate.

fore, the isomerization along the $T_2$ profile is improbable. A feature of the $T_2$ energy profile is that its minimum corresponding to the EAbS minimum is found below the $S_1$ potential energy profile. For the $S_1$ and $T_1$ energy profile, both of them have shallow slope above the area corresponding to the E minimum. The energy barrier along these two pathways is 3.34 and 6.82 kcal/mol, respectively.

As described in these profiles, the possible reaction mechanisms may be attempted to sketch. The photochemical reaction starts with the absorption of light by the EAbS. The $S_2 \leftarrow S_0$ transition is allowed, but isomerization does not occur directly on the $S_2$ state due to the high energy barrier. It requires relaxation to a lower lying excited state when it isomerizes. As shown in Fig. 9b, a direct relaxation from the $S_2$ to $S_1$ state is found to be faster decaying than the $S_2 \leftarrow T_2$ relaxation, and then there exist two pathways: (1) it reaches point A (corresponding to the A in Fig. 9a) along the $S_1$ energy profile in Fig. 9b, then occurs the $S_1 \rightarrow S_0$ intersystem crossing (ISC) to the TS2-Z on the $S_0$ potential energy profile and reaches either the ZAbS or ZAbS′ isomer; (2) it continues relaxing to the $T_1$ state and reaches point B (corresponding to the B in Fig. 9a) along the $T_1$ energy profile in Fig. 9b, then occurs the $T_1 \rightarrow S_0$ intersystem crossing (ISC) but requires a change in spin-multiplicity, and reaches the point TS2-Z on the $S_0$ potential energy profile and reaches either the ZAbS or ZAbS′ isomer. These photochemical isomerization pathways are shown in Fig. 9 with the arrows. These results indicate clearly that the rapid energy redistribution among the various vibrations renders the concentration of such amounts of energy in the inversion coordinate, and thus, the inversion pathway becomes inefficient.

*3.3.2.2. Rotation pathway.* The potential energy profile along the rotation pathway is shown in Fig. 10. For $S_2$ and $T_2$, the potential energy profiles along the rotation pathway have only very steep slopes above the area corresponding to the EAbS minimum and shallow slopes on the ZAbS side. The EAbS → ZAbS energy barrier on $S_2$ and $T_2$ potential energy profile is 26.68 and 42.19 kcal/mol, respectively. These energy barriers are too substantial for isomerization to occur on these two profiles.

The computed $S_1$ potential energy profile starting from the EAbS isomer follows the rotation coordinate and reaches the ZAbS without encountering any barrier. A conical intersection (CI) was found between the $S_0$ and $S_1$ state. The minimum of the $S_1$ state is very close in energy to the maximum along the rotation pathway in the $S_0$ state as can be seen in Fig. 10. For the CI of $S_1/S_0$, the CNNC dihedral angle is about 90°. The $n \rightarrow \pi^*$ excitation resides predominantly along the rotation coordinate. At the CI, the NN and the CN bonds are based on nitrogen σ orbital of intermediate $sp/sp^2$ hybridization, while the lone pair acquires an increased p character. On the other hand, the lone pair of the N atom remains approximately a $sp^2$ orbital at the planar structure. The $S_1$ state is based predominantly on the singly excited configuration $n \rightarrow \pi^*$ along the entire rotation coordinate. It appears that, as the CNNC torsion increases, the coupling between the two nitrogen lone pairs weakens and the $n \rightarrow \pi^*$ excitation tends to localize predominantly on one moiety, that is, the reorganization energy associated with the excitation. Therefore, the two moieties become asymmetric.

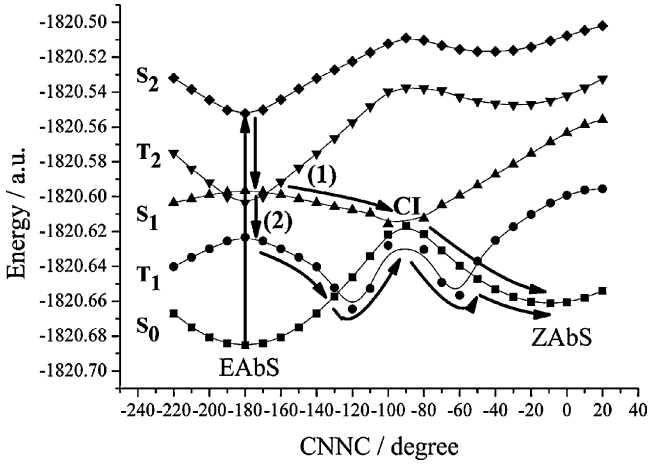


**Fig. 10.** Potential energy profile of the excited state along the CNNC rotational coordinate.

Interestingly, it is found that AbS has an $S_1$–$S_0$ conical intersection along the midpoint of the rotation pathway yet shows a very different quantum yield. This can be explained by looking at the difference in slope on the $S_1$ surface on either side of the conical intersection. The $S_1$ slope above the Z minimum is greater than the corresponding slope on the E side.

It is worth to notice that the maximum of the $T_1$ potential energy profile is not exactly above the $S_0$ barrier, but rather shifted somewhat below the maximum of the $S_0$ potential energy profile. Since the potential energy curves of $S_0$ and $T_1$ cross in the region of rotated CNNC angle, the isomerization can proceed via the rotation route involving the $S_0$–$T_1$–$S_0$ crossing. The crossings between the $T_1$ and $S_0$ potential energy profiles enable the thermal isomerization to proceed via the $T_1 \rightarrow S_0$ intersystem crossing decay. This isomerization is characterized by a lower barrier (0.21 kcal/mol), but requires a change in spin-multiplicity.

The result indicates that the photochemical reaction starts with the absorption of light by the EAbS. The isomerization can easily occur through an excitation to the $S_2$ state. It undergoes a vibration relaxation to the minimum of $S_1$ state and then there exist two pathways (see Fig. 10): (1) followed by descent to either the ZAbS or EAbS conformation via $S_0$–$S_1$ conical intersection; (2) relaxation to the $T_1$ state and descent to the ZAbS conformation via the crossing $S_0$–$T_1$–$S_0$.

## 4. Conclusions

The main purpose of this work is to identify the most efficient isomerization pathway of AbS, and the calculation results clearly demonstrate that its isomerization process may take place in various forms along either the inversion or the rotation pathway. In the $S_0$ state, the thermal isomerization process involves two pathways: the inversion of one CNN angle combined with rotation around the CN bond and the rotation around the CNNC dihedral angle involved inversion of one CNN angle. The thermal isomerization through these two pathways possesses the identical molecular structures at the highest energy points on the potential energy profiles and the energy barriers to be overcome are the same, 20.52 kcal/mol. The calculation results show that the potential energy profile of the former pathway is unusual. It is found that the transition state of the overall reaction is connected to two transition states by the inversion of CNN angle, however, both of the transition states can link to two equivalent ZAbS or two equivalent EAbS, respectively, by the rotation of the CN bond. This pathway is not a simple inversion of the CNN angle, and it can be understood in terms of successive rotation, inversion and rotation processes. The calculations confirm that two phenyl rings of EAbS are in a plane and. ZAbS is the twisted geometry. EAbS isomer is 14.81 kcal/mol lower in energy than ZAbS isomer, thus it is believed that the relative stability of E and Z isomers is not obviously affected by the electron withdrawing substitution compared with Ab. In the $T_1$ state, the EAbS and ZAbS isomers are the twisted geometries, and their energies are higher than that of the $S_0$ state. The isomerization from EAbS to ZAbS only takes place along the rotation pathway around NN bond, of which the energy barrier is 4.11 kcal/mol. This isomerization pro-

cess is characterized by a lower barrier, so the isomerization can occur easily on this state. In the excited states, the $S_2 \leftarrow S_0$ transition is allowed, but isomerization does not occur directly on the $S_2$ state due to the high energy barrier. It need relax to a lower lying excited state when it isomerizes. Along the rotation pathway, the isomerization can be easy descent to either the ZAbS conformation through the $S_0$–$S_1$ conical intersection, and also can proceed via the $S_0$–$T_1$–$S_0$ path involving a change in spin-multiplicity because of a smaller energy barrier. Along the inversion pathway, it need the rapid energy redistribution among the various vibrations renders the concentration of such amounts of energy, so the inversion pathway may be improbable. The results indicate that two mechanisms (inversion and rotation) operate simultaneously for thermal isomerization and it is most like to occur through the rotation pathway for the photochemical isomerization.

## Acknowledgment

This paper was financially supported by the National Natural Science Foundation, 973 Program, PCSIRT and 111 Project.

## References

[1] A.N.-P. Rochon, Chem. Rev. 102 (2002) 4139–4176.
[2] J.A. Delaire, K. Nakatani, Chem. Rev. 100 (2000) 1817–1846.
[3] R.H. Berg, S. Hvilsted, P.S. Ramanujam, Nature 383 (1996) 505–508.
[4] T. Ikeda, O. Tsutsumi, Science 168 (1995) 1873–1875.
[5] T. Muraoka, K. Kinbara, Y. Kobayashi, T.J. Aida, Am. Chem. Soc. 125 (2003) 5612–5613.
[6] A. Harada, Acc. Chem. Res. 34 (2001) 456–464.
[7] V. Balzani, A. Credi, F. Marchioni, J.F. Stoddard, Chem. Commun. 1 (2001) 1860–1861.
[8] R. Ballardini, V. Balzani, A. Credi, M.T. Gandolfi, M. Venturi, Acc. Chem. Res. 34 (2001) 445–455.
[9] V. Balzani, A. Credi, M. Venturi, Coord. Chem. Rev. 171 (1998) 3–16.
[10] I. Willner, S. Rubin, A. Riklin, J. Am. Chem. Soc. 113 (1991) 3321–3325.
[11] L. Ulysse, J. Cubillos, J. Chmielewski, J. Am. Chem. Soc. 117 (1995) 8466–8467.
[12] I.A. Banerjee, L. Yi, H. Matsui, J. Am. Chem. Soc. 125 (2003) 9542–9543.
[13] H. Rau, in: H. Durr, H. Bouas-Lauran (Eds.), Photochromism: Molecular and Systems, Elsevier, Amsterdam, 1990, p. 165.
[14] H. Rau, E. Lüddecke, J. Am. Chem. Soc. 104 (1982) 1616–1620.
[15] S. Monti, G. Orlandi, P. Palmieri, Chem. Phys. 71 (1982) 87–99.
[16] I.K. Lednev, T.-Q. Ye, R.E. Hester, J.N. Moore, J. Phys. Chem. 100 (1996) 13338–13341.
[17] I.K. Lednev, T.-Q. Ye, P. Matousek, M. Towrie, P. Foggi, F.V.R. Neuwahl, S. Umpathy, R.E. Hester, J.N. Moore, Chem. Phys. Lett. 290 (1998) 68–74.
[18] I.K. Lednev, T.-Q. Ye, L.C. Abbot, R.E. Hester, J.N. Moore, J. Phys. Chem. A 102 (1998) 9161–9166.
[19] Y. Hirose, H. Yui, T. Sawada, J. Phys. Chem. A 106 (2002) 3067–3071.
[20] P. Cattaneo, M. Persico, Phys. Chem. Chem. Phys. 1 (1999) 4739–4743.
[21] A.A. Blevins, G.J. Blanchard, J. Phys. Chem. B 108 (2004) 4962–4968.
[22] C.R. Crecca, A.E. Roitberg, J. Phys. Chem. A 110 (2006) 8188–8203.
[23] T. Fujino, T. Tahara, J. Phys. Chem. A 104 (2000) 4203–4210.
[24] T. Fujino, S.Y. Arzhantsev, T. Tahara, J. Phys. Chem. A 105 (2001) 8123–8129.
[25] T. Ishikawa, T. Noro, T. Shoda, J. Chem. Phys. 115 (2001) 7503–7512.
[26] M.L. Tiago, S. Ismail-Beigi, S.G. Louie, J. Chem. Phys. 122 (2005) 94311–94317.
[27] C. Ciminelli, G. Granucci, M. Persico, Chem. Eur. J. 10 (2004) 2327–2341.
[28] E.W.-G. Diau, J. Phys. Chem. A 108 (2004) 950–956.
[29] L. Gagliardi, G. Orlandi, F. Bernardi, A. Cembran, M. Garavelli, Theor. Chem. Acc. 111 (2004) 363–372.
[30] A. Cembran, F. Bernardi, L. Garavelli, L. Gagliardi, G. Orlandi, J. Am. Chem. Soc. 126 (2004) 3234–3243.
[31] S.J. Yeh, H.H. Jaffé, J. Am. Chem. Soc. 81 (1959) 3279–3283.
[32] B. Schmidt, C. Sobotta, S. Malkmus, S. Laimgruber, M. Braun, W. Zinth, P. Gilch, J. Phys. Chem. A 108 (2004) 4399–4404.
[33] M. Hagiri, N. Ichinose, C. Zhao, H. Horiuchi, H. Hiratsuka, T. Nakayama, Chem. Phys. Lett. 391 (2004) 297–301.
[34] L.X. Wang, X.G. Wang, J. Mol. Struct. (THEOCHEM) 806 (2007) 179–186.
[35] L.X. Wang, X.G. Wang, J. Mol. Struct. (THEOCHEM) 847 (2007) 1–9.
[36] L.X. Wang, J. Xu, H.T. Zhou, C.H. Yi, W.L. Xu, J. Photochem. Photobiol. A 205 (2009) 104–108.
[37] L. Briquet, D.P. Vercauteren, J.-M. Andre, E.A. Perpete, D. Jacquemin, Chem. Phys. Lett. 435 (2007) 257–262.
[38] A.M. Chippendale, G. McGeorge, R.K. Harris, C.M. Brennan, Magn. Reson. Chem. 37 (1999) 232–238.
[39] M. Wei, X.F. Tian, J. He, M. Pu, G.Y. Rao, H.L. Yang, L. Yang, T. Liu, D.G. Evans, X. Duan, Eur. J. Inorg. Chem. 2006 (2006) 3442–3450.
[40] M.J. Frisch, G.W. Trucks, H.B. Schlegel, G.E. Scuseria, M.A. Robb, J.R. Cheeseman, J.A. Montgomery Jr., T. Vreven, K.N. Kudin, J.C. Burant, J.M. Millam, S.S. Iyengar, J. Tomasi, V. Barone, B. Mennucci, M. Cossi, G. Scalmani, N. Rega, G.A. Petersson, H. Nakatsuji, M. Hada, M. Ehara, K. Toyota, R. Fukuda, J. Hasegawa, M. Ishida, T. Nakajima, Y. Honda, O. Kitao, H. Nakai, M. Klene, X. Li, J.E. Knox, H.P. Hratchian, J.B. Cross, C. Adamo, J. Jaramillo, R. Gomperts, R.E. Stratmann, O. Yazyev, A.J. Austin, R. Cammi, C. Pomelli, J.W. Ochterski, P.Y. Ayala, K. Morokuma, G.A. Voth, P. Salvador, J.J. Dannenberg, V.G. Zakrzewski, S. Dapprich, A.D. Daniels, M.C. Strain, O. Farkas, D.K. Malick, A.D. Rabuck, K. Raghavachari, J.B. Foresman, J.V. Ortiz, Q. Cui, A.G. Baboul, S. Clifford, J. Cioslowski, B.B. Stefanov, G. Liu, A. Liashenko, P. Piskorz, I. Komaromi, R.L. Martin, D.J. Fox, T. Keith, M.A. Al-Laham, C.Y. Peng, A. Nanayakkara, M. Challacombe, P.M.W. Gill, B. Johnson, W. Chen, M.W. Wong, C. Gonzalez, J.A. Pople, Gaussian 03, Revision B.04, Gaussian, Inc., Pittsburgh, PA, 2003.
[41] N. Kurita, S. Tanaka, S. Itoh, J. Phys. Chem. A 104 (2000) 8114–8120.
[42] C. Zhou, D.M. Birney, Org. Lett. 4 (2002) 3279–3282.
[43] M.A. Silva, J.M. Goodman, Tetrahedron Lett. 46 (2005) 2067–2069.
[44] T. Taketsugu, N. Tajima, K. Hirao, J. Chem. Phys. 105 (1996) 1933–1939.